Optical and Quantum Electronics (2023) 55:593
https://doi.org/10.1007/s11082-023-04846-1

The impact of the spacer and metal layer on the absorption of the heterostructures composed of TMDCs to design narrowband and broadband absorbers

Narges Ansari[1] · **Ensyieh Mohebbi**[1] · **Narges Rezaei**[2]

Received: 19 October 2022 / Accepted: 11 April 2023 / Published online: 14 May 2023

Abstract
Owing to their exceptional optical and electronic properties, the two-dimensional transition metal dichalcogenide (TMDC) monolayers have received a great deal of attention. In fact, it has been suggested that heterostructures including spacers, metals, and two of the TMDC monolayers increase absorption of the narrowband and broadband in the visible range. This study investigates the effects of the number, place, and thickness of the spacers; metal thickness; and angle and polarization of the incident light on the absorption. Inserting the spacer into the structure increases the absorption via inducing light localization and enhancing the intensity of the light in the TMDC monolayers. Further, the effect of employing one spacer on improving the absorption is almost equal to making use of double spacers. The proposed structures by enhanced light-material interaction can raise the amount of the absorption over 90% throughout the broadband wavelength range of 300–480 nm and above 65% at the narrowband wavelength of 617 nm. The findings of the study suggest promising prospects of these structures for a variety of applications particularly in narrowband and broadband optical devices.

Keywords Heterostructures · Narrowband absorber · Broadband absorber · Spacer · TMDC monolayers

1 Introduction

Because of their direct bandgap and high optical absorption in their nanometer thickness, two-dimensional transition metal dichalcogenide (TMDC) monolayers have become an appealing candidate in the visible range, increasingly drawing the attention of the researchers over the recent decade (Soleimani-Amiri and Gholami Rudi 2020; Li and Zhu 2015). TMDCs have a great potential to be adopted in various photonic and optoelectronic devices like photonic absorbers, photodetectors, photovoltaic devices, solar cells, bio-sensors, and

✉ Narges Ansari
n.ansari@alzahra.ac.ir

[1] Department of Atomic and Molecular Physics, Faculty of Physics, Alzahra University, Tehran 1993893973, Iran

[2] Department of Theoretical and Nano Physics, Alzahra University, 1993893973 Tehran, Iran

modulators (Khan et al. 2020; Cheng et al. 2018; Sharma et al. 2020). These materials with the chemical formula of MX_2, where M is a transition metal element from group VI (Mo, W) and X denotes a chalcogen (S, Se) such as MoS_2, $MoSe_2$, WS_2, WSe_2, and the like. These materials form X–M–X with the chalcogen atoms in two hexagonal planes separated by a plane of transition metal atoms. Bulk TMDCs demonstrate a covalently bonded layered structure in which the adjacent layers are held together by weak van der Waals bonding. The bulk TMDCs are semiconductors with an indirect band gap. When the van der Waals bonding is broken by reactions, the material gradually turns into a mono layer with a direct band gap in the visible range (Manzeli et al. 2017; Choi et al. 2017).

Increasing absorption in narrowband, broadband, narrow-angle or broad-angle is the requirement of achieving appropriate optical response in optoelectronical appliances (Ansari et al. 2020a, 2020, 2021). Different methods have been proposed to improve the absorption of TMDCs, e.g., employing multilayer structures containing TMDC monolayers (Strange et al. 2022; Yang et al. 2022). Owing to a variety of absorption peaks of these monolayers, heterostructures consisting of two TMDC monolayers can be used to increase the absorption over a wide range of wavelengths (Ansari et al. 2021). Placing dielectric with a specific thickness as a spacer between TMDCs monolayers is likely to increase the absorption due to its constructive interference (Ansari et al. 2021, 2020c). Placing a metal layer next to TMDC allows reflecting back the incoming light as well as being an architecture for supporting surface plasmons (SPs) or localized surface plasmons (LSPs), to enhance light absorption (Rahman et al. 2020; Luo et al. 2021). Even in the case of using uniform metallic layers in the absorber structure in which no SPs or LSPs find the chance of excitation, metallic layers can act like reflecting mirrors which increase the light path length inside the TMDC layer and increase the light absorption (Li et al. 2017; Cao et al. 2017). Metal type, refractive index and it's work function affect the absorption (Rakić et al. 1998). Au layer has high imaginary refractive index that results in increasing absorption in the wavelength region of 300–500 nm. In terms of experimental work, it is easier to thin Au than other metals. Such absorber can be implemented in light emitting diodes (LEDs) and broadband ultraviolet into near infrared convertors for solar panels. Au is used on connectors and contacts because it has excellent corrosion resistance, high electrical conductivity (only copper and silver are better) and, alloyed with small amounts of nickel or cobalt, has good wear resistance. For low voltage, low current and low contact force applications, Au is the best material (Goodman 2002). For this reason, Au is examined in this article.

The obtained findings of this study suggest that using heterostructures including spacers, metal, and two TMDC monolayers increases the absorption in broadband and narrowband wavelength. In addition, the effects of the number, place, and thickness of the spacers; the thickness of the metal; and angle and polarization of the incident light on absorption have been examined in this study. The results confirm that absorption increases by inserting spacer into the structure inducing localization of light, and resulting in the enhancement of the light intensity in the TMDC monolayers. In sum, the research findings may open the door to potential applications of absorbers and solar cells for enhancing light-material interaction in the visible range.

2 Methods

Heterostructures including metal (Au), spacer (S1, S2), and different combinations of TMDCs in the form of TMDC1/TMDC2, TMDC1/Au/TMDC2, TMDC1/S1/Au/TMDC2, and TMDC1/S1/Au/S2/TMDC2 are investigated to increase light-material

interaction in TMDCs. SiO_2 was chosen as the substrate and SiO_2 or TiO_2 was selected as S1 and S2. The schematic of TMDC1/Au/TMDC2 (structure IV), TMDC1/S1/Au/TMDC2 (structure V), and TMDC1/S1/Au/S2/TMDC2 (structure VI) are shown in Fig. 1,TMDC1 and TMDC2 monolayers are selected from MoS_2, WSe_2, and WS_2 with the thickness of 0.615, 0.649, and 0.618 nm, respectively (Ansari and Ghorbani 2018). The thicknesses of the S1, S2, and Au layers are represented by d_{S1}, d_{S2}, and d_{Au}, respectively. According to Ansari et al., (Ansari et al. 2021), the two combinations of MoS_2/MoS_2 and WS_2/WSe_2 provide the best condition with the optimal absorption. Therefore, we made use of the proposed combinations in the present study. Light passing obliquely through the air was radiated with the incident angle of θ_0 to the structure, and the propagation angle in each layer was obtained according to Snell's law.

Absorption spectra were calculated on the basis of the transfer matrix method (Liu et al. 2012). The transfer matrix of constituted layer for either of the transverse electric (TE) or transverse magnetic (TM) polarizations is obtained as

$$M_j = \begin{pmatrix} \cos\left(2\pi n_j d_j \frac{\cos\theta_j}{\lambda}\right) & -i\,\Gamma \sin\left(2\pi n_j d_j \frac{\cos\theta_j}{\lambda}\right) \\ -i\,\Gamma \sin\left(2\pi n_j d_j \frac{\cos\theta_j}{\lambda}\right) & \cos\left(2\pi n_j d_j \frac{\cos\theta_j}{\lambda}\right) \end{pmatrix}, \quad (1)$$

where n_j, θ_j, and dj are, refractive index, light propagation angle, and thickness of the j^{th} layer, respectively, and λ is the light wavelength on the air and Γ for TE and TM polarizations is correspondingly defined as $\frac{1}{n_j \cos\theta_j}$ and $\frac{\cos\theta_j}{n_j}$. Multiplying tranfer matrix of each constituent layer can make the final transfer matrix M for the whole structure. The tangential electric and magnetic fields can be expressed for the first (E_{0t}, H_{0t}) and last (E_{st}, H_{st}) surrounding layers as follows

$$\begin{pmatrix} E_{st}(z) \\ H_{st}(z) \end{pmatrix} = (M) \begin{pmatrix} E_{0t}(0) \\ H_{0t}(0) \end{pmatrix}, \quad (2)$$

and amplitudes of the transmitted (c^+) and reflected (c^-) fields in each layer are calculated as

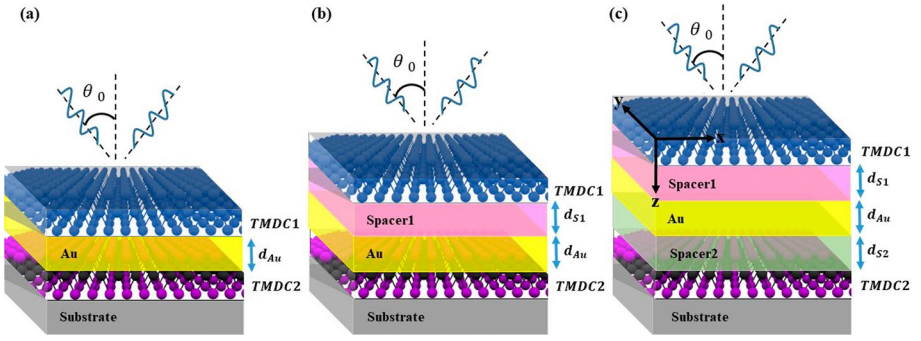

Fig. 1 The heterostructures include TMDC1, TMDC2, metal (Au), and spacer (S1, S2) **a** TMDC1/Au/TMDC2, **b** TMDC1/S1/Au/TMDC2, and **c** TMDC1/S1/Au/S2/TMDC2

$$\begin{pmatrix} E_{0t}(z) \\ H_{0t}(z) \end{pmatrix} = \begin{pmatrix} \psi e^{i2r\pi n_0 \frac{\cos\theta_0}{\lambda}} & \psi e^{-i2r\pi n_0 \frac{\cos\theta_0}{\lambda}} \\ n_0 \varphi e^{i2r\pi n_0 \frac{\cos\theta_0}{\lambda}} & -n_0 \varphi e^{-i2r\pi n_0 \frac{\cos\theta_0}{\lambda}} \end{pmatrix} \begin{pmatrix} c_0^+ \\ c_0^- \end{pmatrix}, \tag{3}$$

$$\begin{pmatrix} E_{st}(z) \\ H_{st}(z) \end{pmatrix} = \begin{pmatrix} \psi e^{i2r\pi n_s \frac{\cos\theta_s}{\lambda}} & \psi e^{-i2r\pi n_s \frac{\cos\theta_s}{\lambda}} \\ n_s \varphi e^{i2r\pi n_s \frac{\cos\theta_s}{\lambda}} & -n_s \varphi e^{-i2r\pi n_s \frac{\cos\theta_s}{\lambda}} \end{pmatrix} \begin{pmatrix} c_s^+ \\ 0 \end{pmatrix}, \tag{4}$$

where 0 and s refer to air and substrate, and ψ and φ for the TE (TM) polarization are equal to $cos\theta_j$ (1) and 1 ($cos\theta_j$), respectively. Next, transmission, reflection, and absorption are determined as follows $T = \frac{n_s \cos\theta_s}{n_0 \cos\theta_0} \left| \frac{c_s^+}{c_0^+} \right|^2$, $R = \left| \frac{c_0^-}{c_0^+} \right|^2$, and A = 1–T–R. The refractive index of SiO_2, TiO_2, Au, and TMDCs monolayer are obtained using formulas $n_{SiO_2} = \sqrt{1.28604141 + \frac{1.07044083\lambda^2}{(\lambda\times10^{-3})^2 - 1.00585997\times10^{-2}} + \frac{1.10202242\lambda^2}{(\lambda\times10^{-3})^2 - 100}}$, (Ghosh 1999) $n_{TiO_2} = \sqrt{5.913 + \frac{0.2441}{\lambda^2 - 0.0803}}$ (DeVore 1951) $N_{Au} = \sqrt{1 - \frac{\omega_p^2}{\omega^2 + i\gamma\omega}}$, (Johnson and Christy 1972) and $N_{TMDC} = n + ik = \sqrt{\varepsilon_{\mathrm{TMDC}}} = \sqrt{(\varepsilon_{real} + i\varepsilon_{imag})} = \sqrt{\varepsilon_\infty + \sum_{j=1}^{N} \frac{a_j}{\omega_j^2 - \omega^2 - i\omega b_j}}$, where λ, ε_∞, ω_p, γ, and ω are the light wavelength in nanometers, DC permittivity, plasma frequency, damping frequency, and incident light frequency, respectively, and a_j, ω_j, and b_j are oscillation power, resonant frequency, and damping factor of the j^{th} oscillator whose quantities are expressed in Ref. (Ansari and Ghorbani 2018). Parameters ε_∞, a_j, ω_j, and b_j for the TMDC monolayers are listed in Table 1.

3 Result

The effects of the thickness of the Au layer as well as the thickness, substance, and number of the spacer layers in the heterostructures including TMDCs on the absorption are examined here. At first, WS_2 and WSe_2 monolayers were selected as TMDC1 and TMDC2. To achieve the aim, an Au layer was placed between the WS_2 and WSe_2 monolayers (structure

Table 1 Coefficients aj, bj, and ωj Correspond to the Lorentz Model for Four Monolayers of WSe_2, MoS_2, and WS_2

	MoS_2			WS_2			WSe_2		
	ω_j(eV)	a_j(eV^2)	b_j(eV)	ω_j(eV)	a_j(eV^2)	b_j(eV)	ω_j(eV)	a_j(eV^2)	b_j(eV)
ε_∞	2.2			7.449			0.05		
1	1.865	0.950	0.072	2.011	1.870	0.029	1.646	0.505	0.036
2	2.008	2.000	0.120	2.404	3.550	0.186	2.426	5.990	0.260
3	2.868	36.54	0.380	2.834	8.416	0.225	2.068	0.885	0.118
4	2.275	11.00	1.000	3.131	42.80	0.639	2.895	16.00	0.344
5	3.745	100.0	0.400				2.200	1.500	0.300
6							2.630	1.850	0.300
7							3.800	60.00	0.700
8							5.000	100.0	0.700

IV) and its absorption was plotted as a function of Au thicknesses and the wavelength, as displayed in Fig. 2a. According to Fig. 2a, an absorption of 60.2%, is observed at λ = 444 nm and d_{Au} = 65 nm and an absorption of 18.6% is detected at λ = 617 nm and d_{Au} = 16 nm. The skin depth of Au layer is between 10 ~ 15 nm for wavelength of 300 to 500 nm. When the thickness of the Au layer is several times the skin depth of Au, the light does not reach the TMDC layer. Further, we selected SiO_2 as spacer1 and placed it between WS_2 monolayer and Au (structure V11),the curve of the absorption versus Au and spacer thicknesses at λ = 444 nm is depicted in Fig. 2b. Optimal absorption in this structure is 92% which is observed when d_{Au} = 65 nm and d_{S1} = 40 nm. Moreover, the curve of the absorption versus Au and spacer thicknesses at λ = 617 nm is displayed in Fig. 2c (structure V21). The optimal amount of absorption at this wavelength is 62% which is observed when d_{Au} = 43 nm and d_{S1} = 67 nm.

Figure 2d displays the absorption at λ = 444 nm, as the function of the spacer1 and spacer2 thickness, for the structure VI13 (in which spacer TiO_2 was placed between WS_2 monolayer and Au and spacer SiO_2 was put between Au and WSe_2 monolayer). The maximum absorption of 96.5% is observed when d_{Au} = 65 nm , d_{S1} = 21 nm, and d_{S2} = 56 nm. The absorption behavior at the wavelength of 617 nm resembles the one at the wavelength of 444 nm.

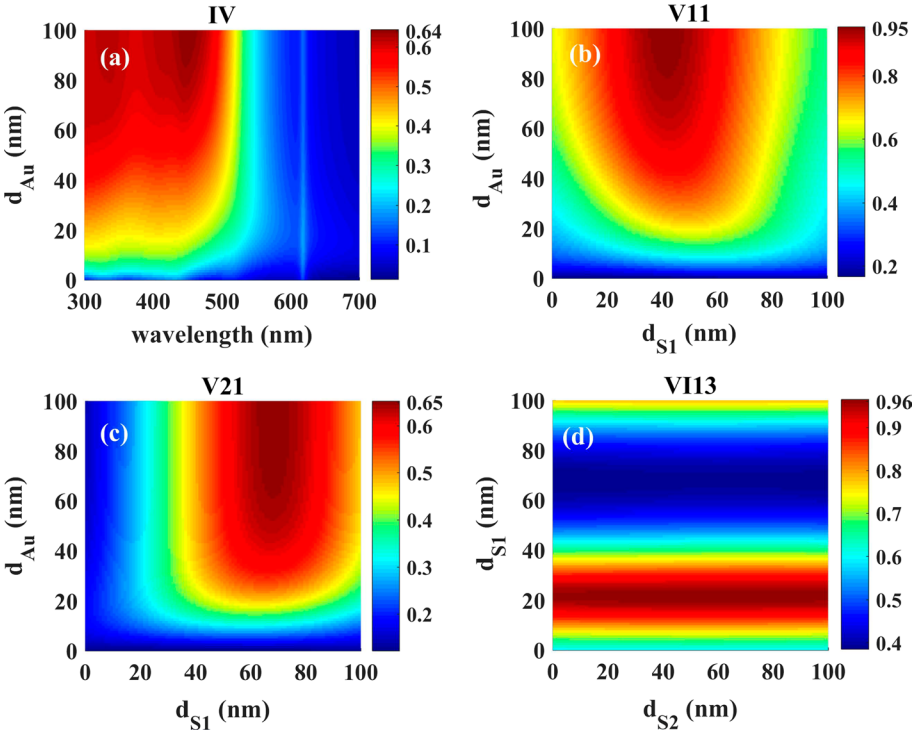

Fig. 2 **a** Absorption of structure IV as a function of Au thicknesses and the wavelength. **b** Absorption spectra of structure V11 versus Au and spacer thicknesses in λ = 444 nm. **c** Absorption spectra of structure V21 versus Au and spacer thicknesses in λ = 617 nm. **d** The absorption as a function of the thicknesses of the spacer1 and spacer2 for structure VI13 at λ = 444 nm

To compare the optimal thicknesses for maximum absorption at the wavelength of 444 nm (617 nm), absorption spectra of the structures as the function of the wavelength are plotted in the Fig. 3a, b. A narrowband wavelength at 617 nm and the broadband wavelength range of 300–480 nm can be observed in this figure. Structures consisting of one spacer and two spacers are displayed by a line and a dashed line, respectively. Absorption of the different combinations for optimal thicknesses of Au, spacer1, and spacer2 at the narrowband wavelength of 617 nm and the broadband wavelength range of 300–480 nm are listed in Table 2. In Fig. 1a, a general schematic of the structure IV is shown. The number after the IV (indicated as " IV1" and " IV2") is a representative of Au layer that has different thicknesses (for example IV1 that means Au layer has thickness equal to 65 nm while IV2 indicates that Au layer has thickness equal to16 nm). Also, structure V and VI are shown in Fig. 1b, c. The first number after the V and VI (indicated as "V12" and "VI11") stands for Au layer with different thicknesses (for V12 $d_{Au} = 66nm$ while for V22 $d_{Au} = 52nm$). Here, the second number represents spacer layer (1 indicates SiO_2 and 2 indicates TiO_2). Thus, V22 is for Au layer with thickness equal to 52 nm and spacer is TiO2 or VI11 addresses Au layer thickness is 46 nm and spacer is SiO_2. Figure 1 shows a general configuration as schematics of the structures in V11, V21 can be the same and their difference is in the spacer type and thickness. This naming is placed in the second column in Tables 2 and 3. This nomenclature of samples is written for when WS_2 and WSe_2 monolayers were selected as TMDC1 and TMDC2 (addressed in Table 2, and if MoS_2 and MoS_2 monolayers were selected as TMDC1 and TMDC2, only the thickness of Au layer is

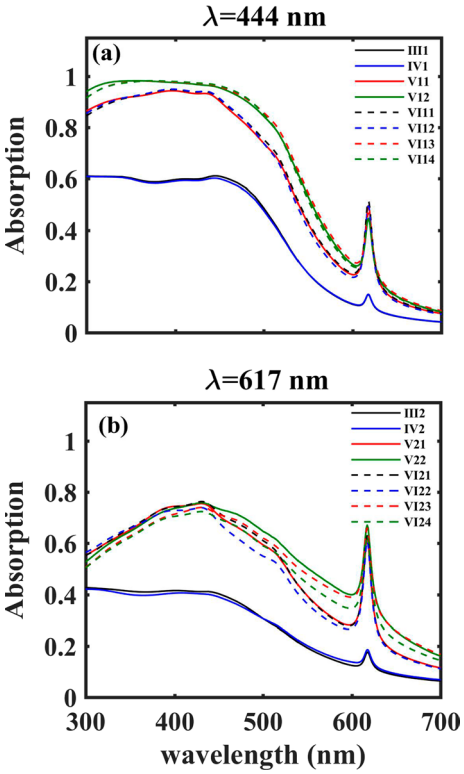

Fig. 3 Absorption spectra as function of wavelength for thicknesses where the absorption is increased at wavelength **a** 444 nm, **b** 617 nm for WS_2 and WSe_2 monolayers were selected as TMDC1 and TMDC2. (Color figure online)

Table 2 Absorption of different combinations in narrowband wavelength at 617 nm and broadband wavelength in 300–480 nm for optimal thickness of Au, spacer1, and spacer2

Structure		S1	S2	Color	d_{Au}(nm)	d_{S1}(nm)	d_{S2}(nm)	A (λ = 617 nm) (%)	A (Wavelength range 300–480 nm) (%)
WS_2	I	–	–	–	–	–	–	11.3	up 1.5
WS_2/WSe_2	II	–	–	–	–	–	–	12.8	up 9.6
WS_2/Au	III1	–	–	Black line	69	–	–	14.8	up 56.2
	III2	–	–	Black line	18	–	–	17.6	up 35.4
WS_2/Au/WSe_2	IV1	–	–	Blue line	65	–	–	15	up 55.0
	IV2	–	–	Blue line	16	–	–	18.6	up 34.5
WS_2/S_1/Au/WSe_2	V11	SiO_2	–	Red line	65	40	–	49.5	up 81.0
	V12	TiO_2	–	Green line	66	20	–	44.6	up 90.3
	V21	SiO_2	–	Red line	43	67	–	62	up 55.3
	V22	TiO_2	–	Green line	52	35	–	67.1	up 52.7
WS_2/S_1/Au/S_2/WSe_2	VI11	SiO_2	SiO_2	Black dashed line	65	42	59	51.3	up 82.3
	VI12	SiO_2	TiO_2	Blue dashed line		41	64	49.3	up 82.2
	VI13	TiO_2	SiO_2	Red dashed line		21	56	46.6	up 91.2
	VI14	TiO_2	TiO_2	Green dashed line		21	64	45.1	up 91.4
	VI21	SiO_2	SiO_2	Black dashed line	48	69	58	63	up 55.3
	VI22	SiO_2	TiO_2	Blue dashed line		67	27	60.9	up 56.4
	VI23	TiO_2	SiO_2	Red dashed line		36	46	66	up 50.6
	VI24	TiO_2	TiO_2	Green dashed line		36	62	63.0	up 50.4

Table 3 Absorption of different combinations in narrowband wavelength at 617 nm and broadband wavelength in 300–480 nm for optimal thickness of Au, spacer1, and spacer2

Structure		S1	S2	Color	d_{Au} (nm)	d_{S1} (nm)	d_{S2} (nm)	A ($\lambda = 617$ nm) (%)	A (Wavelength range 300–480 nm) (%)
MoS_2	I	–	–	–	–	–	–	5.4	up 7.0
MoS_2/MoS_2	II	–	–	–	–	–	–	10.0	up 12.5
MoS_2/Au	III	–	–	Black line	54	–	–	11.8	up 52.8
	III2	–	–	Black line	20	–	–	13.8	up 38.3
MoS_2/Au/MoS_2	IV1	–	–	Blue line	65	–	–	11.5	up 54.2
	IV2	–	–	Blue line	15	–	–	16.1	up 34.6
MoS_2/S_1/Au/MoS_2	V11	SiO_2	–	Red line	46	29	–	26.1	up 72.6
	V12	TiO_2	–	Green line	47	16	–	26.6	up 77.9
	V21	SiO_2	–	Red line	29	63	–	39.0	up 61.2
	V22	TiO_2	–	Green line	43	35	–	48.0	up 57.8
MoS_2/S_1/Au/S_2/MoS_2	VI11	SiO_2	SiO_2	Black dashed line	46	31	47	27.1	up 76
	VI12	SiO_2	TiO_2	Blue dashed line		31	46	24.4	up 71.2
	VI13	TiO_2	SiO_2	Red dashed line		16	44	26.5	up 79.6
	VI14	TiO_2	TiO_2	Green dashed line		16	46	23.0	up 75.9
	VI21	SiO_2	SiO_2	Black dashed line	36	65	67	41.0	up 61.6
	VI22	SiO_2	TiO_2	Blue dashed line		52	18	37.0	up 63.9
	VI23	TiO_2	SiO_2	Red dashed line		35	61	46.0	up 55.5
	VI24	TiO_2	TiO_2	Green dashed line		32	14	43.0	up 62.1

different that are addressed in Table 3. As shown in Table 2 and Fig. 3a, the absorptions of the structures VI14 and VI13 (structures VI11 and VI12) correspond to each other. The structure VI14 in the wavelength range of 300 to 480 nm shows the maximum absorption. Nevertheless, due to the minute difference between this absorption and that of the structure VI13, among all the structures with double spacers, structure VI13 is selected as the optimal structure with maximum amount of absorption in this wavelength range. Compared to all other structures with one spacer, structure V12 demonstrates the maximum absorption. The maximum absorption of the one spacer (structure V12) is almost equal to that of the double spacers (structure VI13). Thus, considering the fact that fewer layers are more suitable for experimental works, structure V12 is selected as the best structure in this wavelength range. Examining the absorption at the peak of 617 nm, reveals that the structure with a spacer, structure VI11, is the superior structure with the maximum absorption.

According to Table 2 and Fig. 3b, structure V21 in the broadband wavelength range of 300–480 nm and structure V22 at the narrowband wavelength of 617 nm are selected as the best options demonstrating maximum absorption. Comparing Fig. 3a, b reveals that structure V12 (the green line in Fig. 3a and structure V22 (the green line in Fig. 3b are superior options for designing broadband and narrowband wavelength, respectively.

Another combination that increases the absorption is the placement of MoS_2 monolayer, instead of TMDC1 and TMDC2, in the structures. An Au layer was placed between the two MoS_2 monolayers (structure IV) and its absorption was plotted as a function of Au thicknesses and the wavelength, as displayed in Fig. 4a. According to the Fig. 4a, an absorption is 68.3% is observed at $\lambda = 349$ nm and $d_{Au} = 65$ nm and an absorption of 16.1% is detected at $\lambda = 617$ nm and $d_{Au} = 15$ nm. By selecting SiO_2 as spacer1 and placing its between MoS_2 and the Au monolayer (structure V11), the curve of the absorption versus Au and spacer thicknesses at $\lambda = 349$ nm is depicted in Fig. 4b. Optimal absorption in this structure is 96% which is observed when $d_{Au} = 46$ nm and $d_{S1} = 29$ nm. Moreover, the curve of the absorption versus Au and spacer thicknesses at $\lambda = 617$ nm is displayed in Fig. 4c (structure V21). The optimal amount of absorption at this wavelength is 39% which is observed when $d_{Au} = 29$ nm and $d_{S1} = 63$ nm. Figure 4d displays the absorption at $\lambda = 349$ nm, as the function of the spacer1 and spacer2 thickness, for the structure VI13 (in which spacer TiO_2 was placed between MoS_2 monolayer and Au and spacer SiO_2 was put between Au and MoS_2 monolayer). The maximum absorption of 94.5% is observed when $d_{Au} = 46$ nm,$d_{S1} = 16$ nm, and $d_{S2} = 44$ nm. The absorption behavior at the wavelength of 617 nm resembles the one at the wavelength of 349 nm.

To compare the optimal thicknesses for maximum absorption at the wavelength of 349 nm (617 nm), absorption spectra of the structures as the function of the wavelength are plotted in the Fig. 5a, b. A narrowband wavelength at 617 nm and the broadband wavelength range of 300–480 nm can be observed in this figure. Structures consisting of one spacer and two spacers are displayed by a line and a dashed line, respectively. Absorption of the different combinations for optimal thicknesses of Au, spacer1, and spacer2 at the narrowband wavelength of 617 nm and the broadband wavelength range of 300–480 nm are listed in Table 3. As shown in Table 3 and Fig. 5a, nevertheless, due to the minute difference between this absorption and that of the structure VI13, among all the structures with double spacers, structure VI13 is selected as the optimal structure with maximum amount of absorption in this wavelength range. Compared to all other structures with one spacer, structure V12 demonstrates the maximum absorption. The maximum absorption of the one

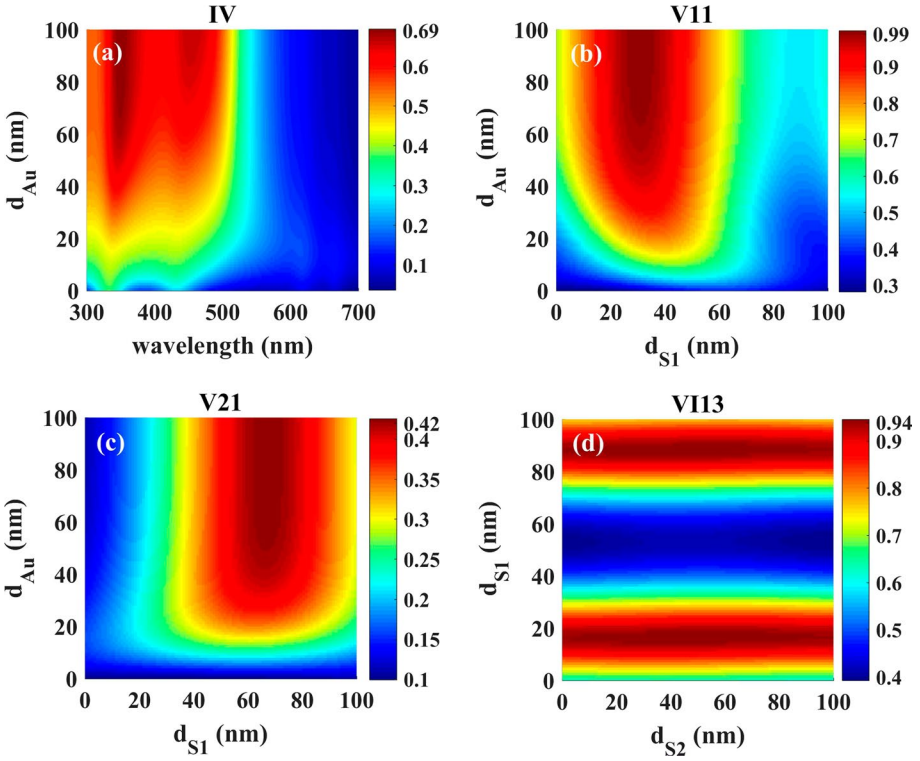

Fig. 4 **a** Absorption structure IV as a function of Au thicknesses and wavelength. **b** Absorption spectra structure V11 versus Au and spacer thicknesses in λ = 349 nm. **c** Absorption spectra structure V21 versus Au and spacer thicknesses in λ = 617 nm. **d** The absorption as a function of the thicknesses of the spacer1 and spacer2 for structure VI13 at λ = 349 nm

spacer (structure V12) is almost equal to that of the double spacers (structure VI13). Thus, considering the fact that fewer layers are more suitable for experimental works, structure V12 is selected as the best structure in this wavelength range. Examining the absorption at the peak of 617 nm, reveals that the structure with a spacer, structure V12, is the superior structure with the maximum absorption.

According to Table 3 and Fig. 5b, similar to Fig. 5a, the structure V21 in the broadband wavelength of 300–480 nm and the structure V22 at the narrowband wavelength of 617 nm are selected as the best structures with the maximum absorption. Comparing Fig. 5a, b, reveals that the structure V12(the green line in Fig. 5a is the superior option for designing broadband wavelength and structure V22 (the green line in Fig. 5b is the better choice for designing narrowband wavelength.

The intensity versus position curves of the structures IV1, V11, V12, and VI13, in which WS_2 and WSe_2 monolayers were respectively selected as TMDC1 and TMDC2 at the wavelength of 444 nm are displayed in Fig. 6a–d. The spacer layer localized the light

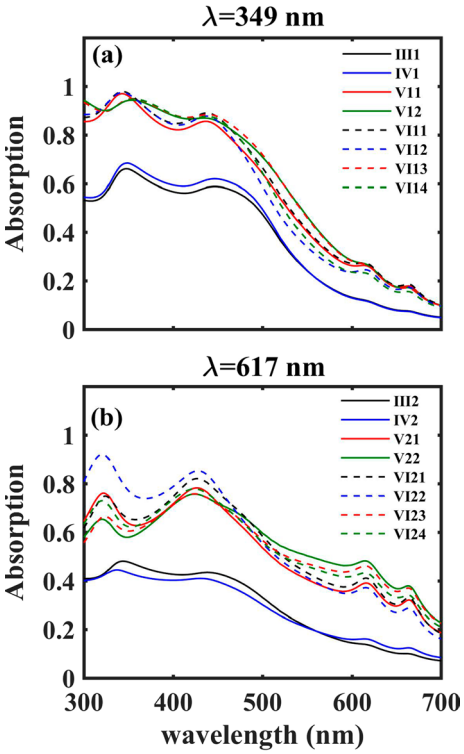

Fig. 5 Absorption spectra for chosen structures as function of wavelength for thicknesses where the absorption is increased at wavelength **a** 349 nm, **b** 617 nm for MoS_2 and MoS_2 monolayers were selected as TMDC1 and TMDC2

in the WS_2 monolayer. The intensity of the WS_2 monolayer in the structure V11 is greater than that in other structures. Structures V11, V12, and VI13 show the highest amounts of absorption which are almost the same.

Similarly, the intensity versus position curves of the structures IV1, V11, V12, and VI13, in which MoS_2 monolayer is selected as both TMDC1 and TMDC2 at the wavelength of 349 nm are presented in Fig. 7a–d. The intensity of the MoS_2 monolayer in the structure V11 is greater than that in other structures. Therefore, structure V11 demonstrates the maximum absorption. Improvement of the absorption should be attributed to the localization of the light as well as light intensity enhancement of the MoS_2 monolayer.

To study the effect of polarization and incident angle, the absorption versus wavelength and light incident angle was depicted for both of the transverse electric (TE) and transverse magnetic (TM) polarization. This depiction is based on the data provided in Tables 2 and 3 for the structure V22, when WS_2 and WSe_2 were respectively chosen as TMDC1 and TMDC2 Fig. 8a, b and MoS_2 was selected as both TMDC1 and TMDC2 Fig. 8c, d. According to Fig. 8a, b, absorption peak at 617 nm is not sensitive to the angle and polarization of

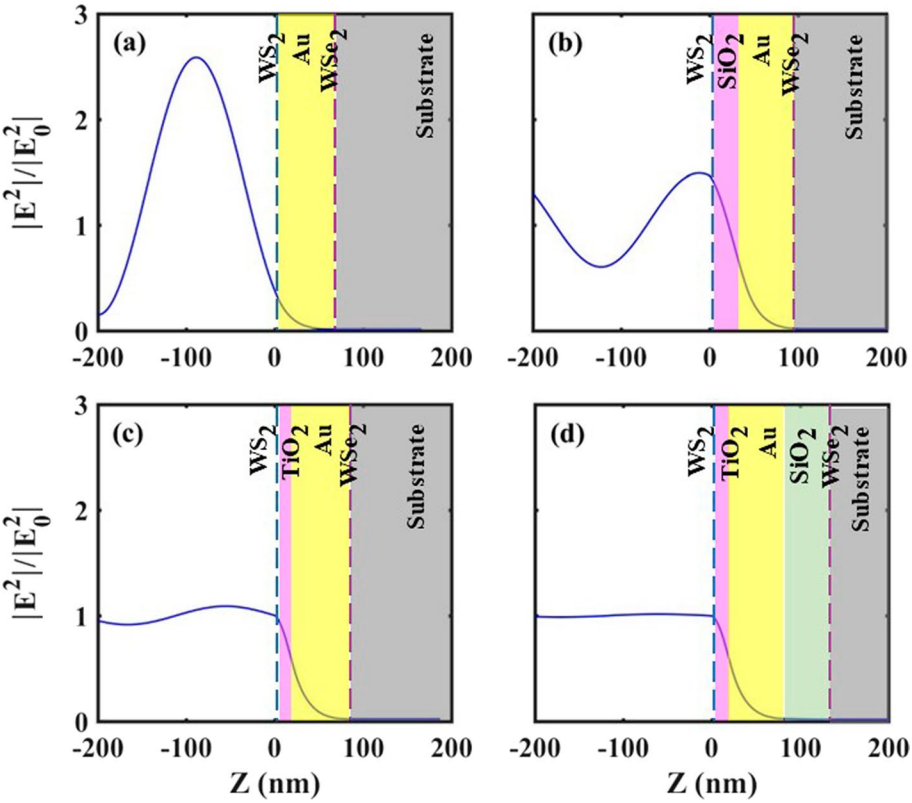

Fig. 6 The intensity versus position at the wavelength of 444 nm for structures **a** IV1, **b** V11, **c** V12, and **d** VI13 that TMDC1 and TMDC2 are selected WS_2 and WSe_2 monolayers

the incident light and narrowband absorption is fixed, which can be useful for the devices which need to be insensitive to the incident angle (tolerance). However, over the wavelength range of 400–455 nm, absorption depends on the angle and polarizations of the incident light and the absorption widths above 70% are observed in the angle range of 0°–53°. Notwithstanding, by increasing the incident angle in Fig. 8c, d, the peak at 617 nm disappears and the absorption in the broadband wavelength range becomes dependent on the angle and polarization. The absorption above 70% for TE (TM) polarization is observed in the wavelength range of 400–460 nm and angle range of 0 to 46° (0°–70°).

Finally, the studied structure is compared with other articles and the results are given in the Table 4.

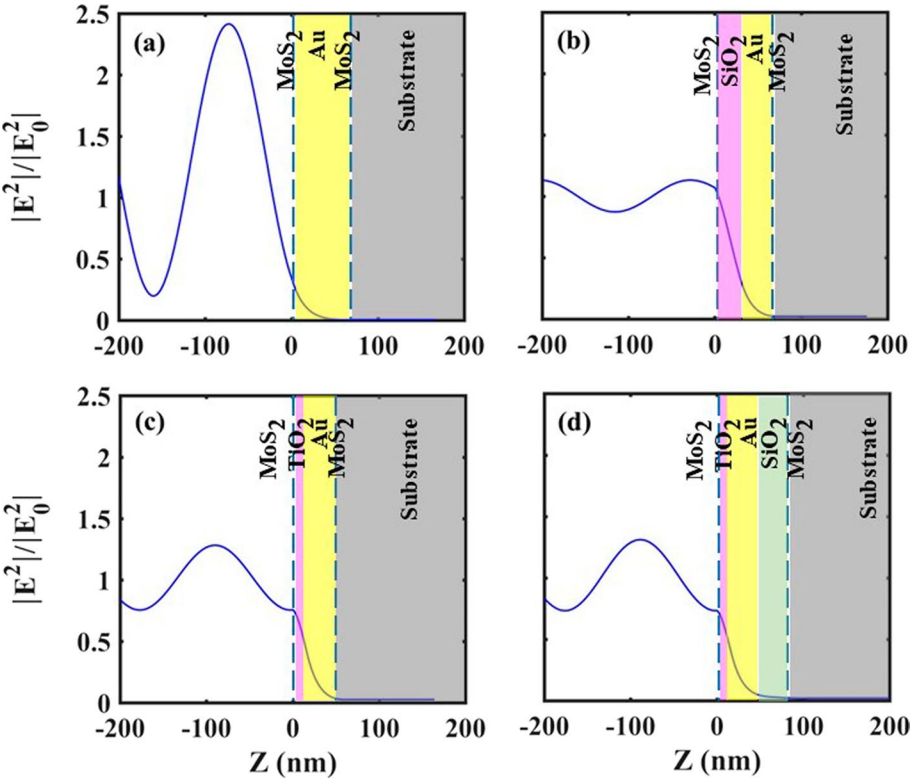

Fig. 7 The intensity versus position at the wavelength of 349 nm for structures **a** IV1, **b** V11, **c** V12, and **d** VI13 that TMDC1 and TMDC2 are chosen MoS2 monolayer

4 Conclusions

Findings of this study suggest that heterostructures including spacers, metal, and two TMDC monolayers in the visible range achieve high absorption in broadband and narrowband wavelength range. In addition, the effects of the type of TMDC; the number, place, and thickness of the spacers; metal thickness; and the angle and polarization of the incident light on the amount of absorption and peak wavelength were explored in this study. It was found that maximum amounts of absorption in the structures with one spacer are almost equal to those in the structures with double spacers. Further, the results of the current study affirms that absorption increases due to the localization and enhancement of the

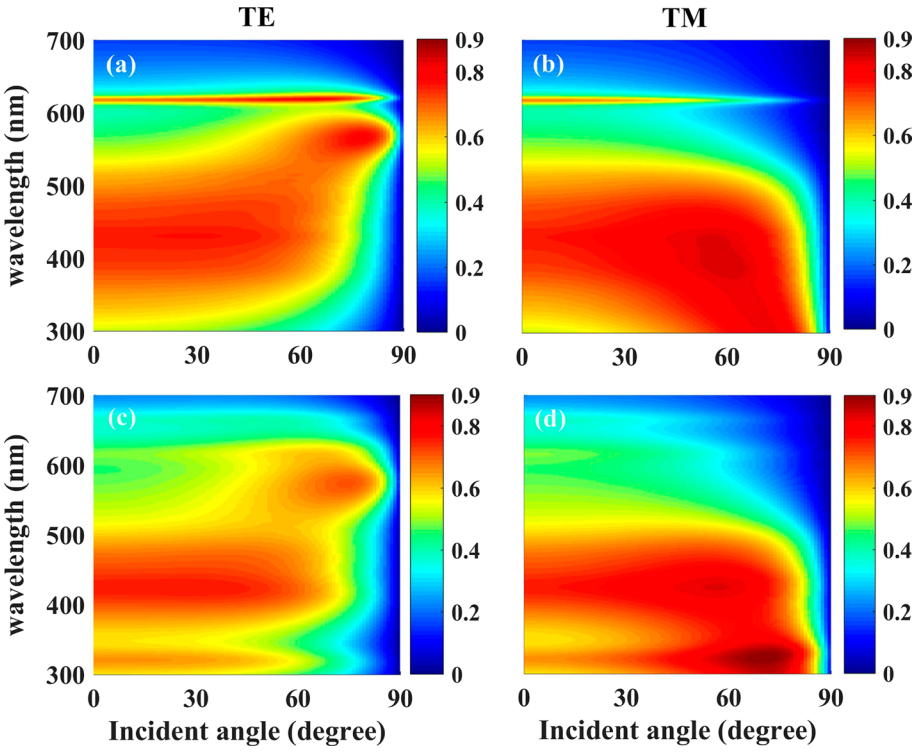

Fig. 8 Absorption spectra versus light incident angle for the data in Tables 2 and 3 for structure V22 when WS_2 and WSe_2 chosen as TMDC1 and TMDC2 for both **a** TE and **b** TM polarization and when MoS_2 was selected as both TMDC1 and TMDC2 for both **c** TE and **d** TM polarization

light intensity in the TMDC monolayers induced by inserting a spacer into the structure. In fact, the proposed structure increases absorption over 90% in broadband and above 65% in the narrowband wavelength range. Moreover, the absorption peak of the structure containing WS_2 at 617 nm is not sensitive to the angle and polarization of the incident light. The proposed structures have implications for designing methods to improve light-matter interaction in broadband and narrowband wavelength ranges.

Table 4 Absorption maximum and wavelength range in which absorption maximum structures studied in similar articles

Structure	TMDC1 MoS_2	TMDC2 MoS_2	TMDC1 WSe_2	TMDC2 WS_2
TMDC1/TMDC2 (Ansari et al. 2021)				
absorption at 617 nm	–		19%	
Absorption width	424–438 nm		419–438 nm	
	26%		19%	
TMDC1/S_1/TMDC2 (Ansari et al. 2021)				
absorption at 617 nm	–		24%	
Absorption width	431–433 nm		424–437 nm	
	35%		23%	
TMDC1/S_1/TMDC2/S_2 (Ansari et al. 2021)				
absorption at 617 nm	–		31%	
Absorption width	429–435 nm		429–436 nm	
	44%		32%	
TMDC1/S_1/Au (Ansari et al. 2020c)				
absorption at 619 nm	–		61%	
Absorption width	–		–	
TMDC1/Au/S_1/Si (Ansari et al. 2020d)				
absorption at 429 nm	99%		–	
Absorption width	300–447 nm		–	
	94%			
TMDC1/S_1/Au/S_2/TMDC2				
absorption at 617 nm	48%		67.1	
Absorption width	300–480 nm		300–480 nm	
	77.9%		90.3%	

Authors' contributions Ansari: Supervision, Editing, Conceptualization, Methodology, Investigation, Visualization. Mohebbi: Conceptualization, Methodology, Software, Data curation, preparation, Editing, Visualization, Investigation. Rezaei: Software.

Funding Not applicable.

Availability of data and materials Not applicable.

Declarations

Competing interests The authors declare no competing interests.

Ethical approval Not applicable.

References

Ansari, N., Ghorbani, F.: Light absorption optimization in two-dimensional transition metal dichalcogenide van der Waals heterostructures. JOSA B (2018). https://doi.org/10.1364/JOSAB.35.001179

Ansari, N., Mohebbi, E., Mohammadi, S.: Ultra-narrowband wavelength adjustable multichannel near perfect absorber in Thue-Morse defective quasi-photonic crystals embedded with MoS2 monolayer. J. Appl. Phys. (2020). https://doi.org/10.1063/5.0011881

Ansari, N., Mohebbi, E., Fallah, K.: Ultra-broadband and broad-angle absorbers with transition metal dichalcogenide monolayer using Thue-Morse quasi-photonic crystals. Opt. Mater. (2020a). https://doi.org/10.1016/j.optmat.2020.110039

Ansari, N., Mohebbi, E., Gholami, F.: Enhancement of light absorption in a WS_2 monolayer using spacer and Au layers. J. Appl. Phys. (2020c). https://doi.org/10.1063/1.5131699

Ansari, N., Mohebbi, E., Gholami, F.: Nearly perfect and broadband optical absorption by TMDCs in cover/TMDC/spacer/Au/substrate multilayers. Appl. Phys. B (2020d). https://doi.org/10.1007/s00340-019-7352-3

Ansari, N., Goudarzi, B., Mohebbi, E.: Design of narrowband or broadband absorber by heterostructures including TMDCs and spacers. Opt. Laser Technol. (2021). https://doi.org/10.1016/j.optlastec.2020.106771

Cao, J., et al.: Enhancement of broad-band light absorption in monolayer mos2 using ag grating hybrid with distributed bragg reflector. Superlattices Microstruct. **110**, 26–30 (2017). https://doi.org/10.1016/j.spmi.2017.09.008

Cheng, J., Wang, C., Zou, X., Liao, L.: Recent advances in optoelectronic devices based on 2D materials and their heterostructures. Adv. Opt. Mater. (2018). https://doi.org/10.1002/adom.201800441

Choi, W., Choudhary, N., Han, G.H., Park, J., Akinwande, D., Lee, Y.H.: Recent development of two-dimensional transition metal dichalcogenides and their applications. Mater. Today. (2017). https://doi.org/10.1016/j.mattod.2016.10.002

DeVore, J.R.: Sensitive 4-aminoantipyrine method for phenolic compounds. JOSA (1951). https://doi.org/10.1364/JOSA.41.000416

Ghosh, G.: Dispersion-equation coefficients for the refractive index and birefringence of calcite and quartz crystals. Opt. Commun. (1999). https://doi.org/10.1016/S0030-4018(99)00091-7

Goodman, P.: Current and future uses of gold in electronics. Gold Bull. (2002). https://doi.org/10.1007/BF03214833

Johnson, P.B., Christy, R.W.: Optical constants of the noble metals. Phys. Rev. B. (1972). https://doi.org/10.1103/PhysRevB.6.4370

Khan, K., Tareen, A.K., Aslam, M., Wang, R., Zhang, Y., Mahmood, A., Ouyang, Z., Zhang, H., Guo, Z.: Recent developments in emerging two-dimensional materials and their applications. J. Mater. Chem. C (2020). https://doi.org/10.1039/C9TC04187G

Li, X., Zhu, H.: Two-dimensional MoS2: properties, preparation, and applications. J. Materiom. (2015). https://doi.org/10.1016/j.jmat.2015.03.003

Li, H., et al.: Total absorption of light in monolayer transition-metal dichalcogenides by critical coupling. Opt. Express. (2017). https://doi.org/10.1364/OE.25.031612

Liu, J.T., Liu, N.H., Li, J., Jing Li, X., Huang, J.H.: Enhanced absorption of graphene with one-dimensional photonic crystal. Appl. Phys. Lett. (2012). https://doi.org/10.1063/1.4740261

Luo, G.P., Chen, X.Y., Hu, S.M., Zhu, W.L.: Enhanced light absorption in monolayer tungsten disulfide with dielectric Bragg reflector and metallic thin film. Optik (2021). https://doi.org/10.1016/j.ijleo.2021.166781

Manzeli, S., Ovchinnikov, D., Pasquier, D., Yazyev, O.V., Kis, A.: 2D transition metal dichalcogenides. Nat. Rev. Mater. (2017). https://doi.org/10.1038/natrevmats.2017.33

Rahman, S., Priyam, A.G., Mullah, Z., Basak, A.K.: Performance analysis of light absorption in TMDC monolayers using cover, spacer, gold and VO_2 layers. In: 2020 IEEE international women in engineering (WIE) conference on electrical and computer engineering (WIECON-ECE) (2020). https://doi.org/10.1109/WIECON-ECE52138.2020.9397941

Rakić, A.D., Djurišić, A.B., Elazar, J.M., Majewski, M.L.: Optical properties of metallic films for vertical-cavity optoelectronic devices. Appl. Opt. (1998). https://doi.org/10.1364/AO.37.005271

Sharma, A.K., Kaur, B., Popescu, V.A.: On the role of different 2D materials/heterostructures in fiber-optic SPR humidity sensor in visible spectral region. Opt. Mater. (2020). https://doi.org/10.1016/j.optmat.2020.109824

Soleimani-Amiri, S., Gholami Rudi, S.: Effects of sulfur line vacancy defects on the electronic and optical properties of armchair MoS2 nanoribbon. Opt. Mater. (2020). https://doi.org/10.1016/j.optmat.2020.110491

Strange, L.E., Garg, S., Kung, P., Ashaduzzaman, M., Szulczewski, G., Pan, S.: Electrodeposited transition metal dichalcogenides for use in hydrogen evolution electrocatalysts. J. Electrochem. Soc. (2022). https://doi.org/10.1149/1945-7111/ac4f25

Yang, L., Wang, Z., Zhou, B., Ming, L., Deng, L., Yu, L., Cheng, L.: Approaching multi-band and broadband high absorption based on one-dimensional layered structures containing monolayer MoS2. Phys. Scr. (2022). https://doi.org/10.1088/1402-4896/ac710a